JOURNAL OF APPLIED ELECTROCHEMISTRY 3 (1973) 1–15

The electrochemical characterization of n-type gallium arsenide

T. AMBRIDGE, C. R. ELLIOTT, AND M. M. FAKTOR

Post Office Research Department, Dollis Hill, U.K.

Received 3 August 1972

A method for determining the carrier concentration of n-type gallium arsenide by an electrochemical technique is described. The minority carrier diffusion length is also obtained, and using subsidiary measurements the minority carrier lifetime can be estimated. The extension of this treatment to the characterization of epitaxial layers is discussed.

1. Introduction

There is currently a growing demand for well-characterized epitaxially-grown layer structures of gallium arsenide and other semiconductors for the manufacture of high frequency devices for use in microwave and optical communication systems. Established techniques for the measurement of the electrical properties of grown layers suffer from important practical limitations. Hall effect measurements [1] require that there is electrical isolation between the layer and the substrate, so that n-type layers, for example, can only be characterized if grown on p-type or semi-insulating substrates, whereas device structures of current interest, such as IMPATT and Gunn diodes demand n-type grown layers on n^+ substrates. [2, 3] The technique frequently employed for measurements on the latter type of structure is the differential capacitance-voltage method which is capable in principle of yielding a depth profile of carrier concentration within the epitaxial layer. However, breakdown voltages limit the maximum depth beneath the surface which can be explored, to a value which depends on the doping level (e.g., ~ 20 μm at 10^{15} cm^{-3}, ~ 3 μm at 10^{17} cm^{-3}) [4]. In many cases, for a complete profile to be obtained it is necessary to remove material by repeated controlled step etching prior to electrode deposition.

This procedure is inconvenient, time consuming, and introduces additional sources of error. For these reasons we have considered a fresh approach to the characterization of gallium arsenide device material, based on an electrochemical technique.

It is well known, that there is a striking distinction between the kinetics of electrode reactions for the cases of metal and semiconductor electrodes [5, 6, 7]. In the latter case, provided the electrolyte is sufficiently concentrated, charge transfer may be limited by the availability of carriers from within the electrode material, and virtually the whole of any applied potential between the electrode and electrolyte will be dropped across a space charge region within the semiconductor; i.e., the potential drop in the Gouy-Helmholtz layer in the electrolyte may be neglected. The anodic voltage-current behaviour of a number of n-type gallium arsenide electrodes in an electrolytic cell was therefore investigated with the object of relating it to known electrical properties of these samples. This work confirmed that carrier concentration can be deduced from such measurements, and shows that an additional useful material parameter is obtained. The voltage-current characteristics of an illuminated electrode yield information about a surface region of known finite depth; a continuous process of electrochemical etching and measurements, *in situ*, characterizes the electrical properties as a function of depth.

Printed in Great Britain. © 1973 *Chapman and Hall Ltd.*

2. Experimental

2.1 *Apparatus*

Fig. 1 shows the electrochemical cell designed for this work. Samples were held in place by gold alloy wire springs which also served as electrical contacts, permitting a rapid interchange of samples. A light-pipe was provided to permit illumination of the sample from a variety of light sources. A 10% (w/v) aqueous KOH solution electrolyte was used; the solution was prepared from 'analytical grade' reagent, with minimum exposure to the atmosphere. It was maintained, and pumped through the cell, under a pressure of 'white spot' nitrogen, to minimize oxygen and carbon dioxide contamination. A saturated calomel electrode (SCE) was employed as a reference electrode; contamination of the electrolyte in the region of the sample, by ions from the reference half-cell, was minimized by the cell design. A spectrographically pure carbon electrode was employed as the working cathode.

The electrical measurement circuit for voltage-current characteristic determination is shown in simplified form, in Fig. 2. A potentiostatic system was used to regulate the current passed through the sample, such that the potential between the sample and reference electrode was held close to that set up on a reference voltage source. A Wenking Potentiostat type 61/TR provided the potential balance, and the current supply function, whilst the reference voltage was externally swept over the desired range. In order to eliminate the effect of the resistive potential drop at the sample contact, separate probes were used for current and voltage contacts, and the cell potential was measured independently of the grounded swept voltage source, using a Levell meter, type TM 9BP, as a high impedance voltmeter. A logarithmic microammeter, was incorporated into the circuit, so that semi-logarithmic voltage-current curves could be plotted directly using an x-y recorder. In addition a Time Electronics type TS100A digital integrator was available to measure the time integral of the dissolution current during the anodic stripping of epitaxial layers; this instrument also provided pulse signals to initiate automatic plotting of voltage-log current curves at pre-determined intervals of depth of material removed. Two light sources were provided for optical excitation of samples: a 36 W tungsten filament lamp, and a 10 W potassium discharge lamp (Philips type 93103). Provision was made for the inclusion of optical filters in the light path. To prevent interference from stray light, the electrolytic cell, and lamps, were placed within a large, lightproof box.

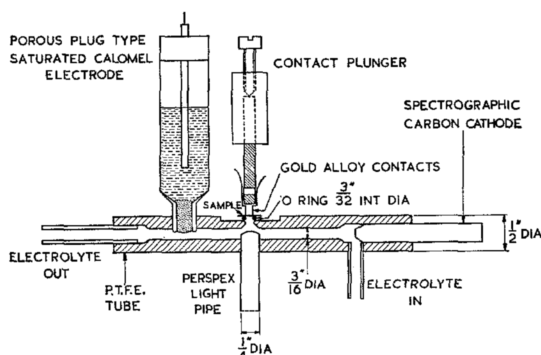

Fig. 1. The electrolytic flow cell.

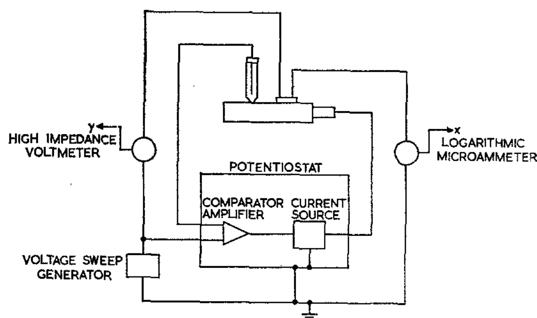

Fig. 2. Circuit block diagram of the potentiostatic system.

2.2 *Materials*

A wide selection of gallium arsenide single crystals was used in order to study the electrochemical voltage-current behaviour as a function of n-type doping level. This selection comprised wafers, about 0·5 mm thick, of boat-grown and Czochralski grown material supplied by Mining and Chemical Products Ltd. (U.K.), Bell and Howell Inc. (U.S.A.), The Royal Radar Establishment (Malvern U.K.), and Monsanto Chemicals Ltd. (U.K.), and a thick (70 μm) epitaxial layer supplied by the latter company. For a study of the anodic stripping of epitaxial layers, the

samples were obtained from the Royal Radar Establishment and the Plessey Company (U.K.). In all cases the surface studied was the (100) plane.

2.3. *Procedure*

Both faces of all bulk gallium arsenide samples were polished using the well-established bromine in methanol chemical-mechanical process [8]. Probe-type Hall effect measurements were carried out to determine carrier concentration and carrier mobility prior to the electrochemical investigations. Epitaxial layers were used as supplied, and manufacturers' electrical data were relied upon.

Before commencing electrochemical experiments, 'white spot' nitrogen was bubbled through the electrolyte reservoir to reduce the amount of dissolved oxygen; this was continued throughout the course of each experiment. An electrolyte flow rate of ·02 ml s^{-1} was then established and electrical probe contacts to the sample were 'formed' by momentary application of 50 V A.C. across the pair; contact resistances of about 100 Ω were typical, as monitored on an oscilloscope. At this stage voltage-log current characteristics of the electrode-electrolyte system could be obtained using the apparatus described. Detailed experiments were invariably preceded by repeatedly automatically plotting characteristics with the sample under illumination, until these were entirely reproducible. This procedure typically involved the electrochemical removal of a few tens of nm of material from the sample.

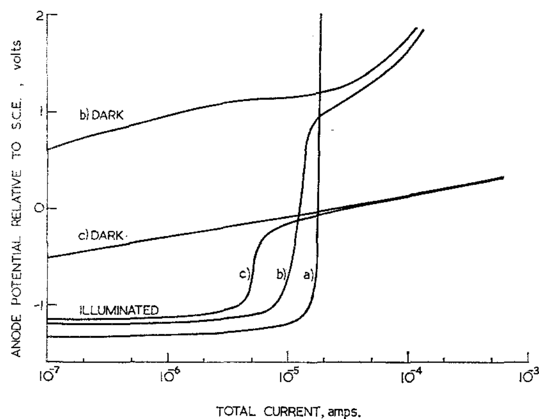

Fig. 3. Voltage-current characteristics in the dark and under constant potassium lamp illumination: (a) Sample No. 2, $3{\cdot}75\times10^{15}$ electrons cm^{-3}; (b) Sample No. 4, $3{\cdot}81\times10^{16}$ electrons cm^{-3}; (c) Sample No. 12, $1{\cdot}90\times10^{18}$ electrons cm^{-3}.

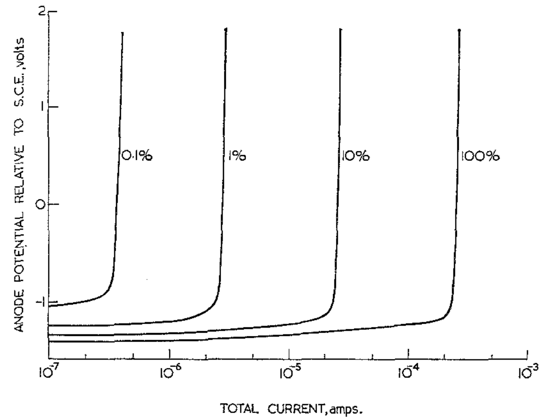

(a)

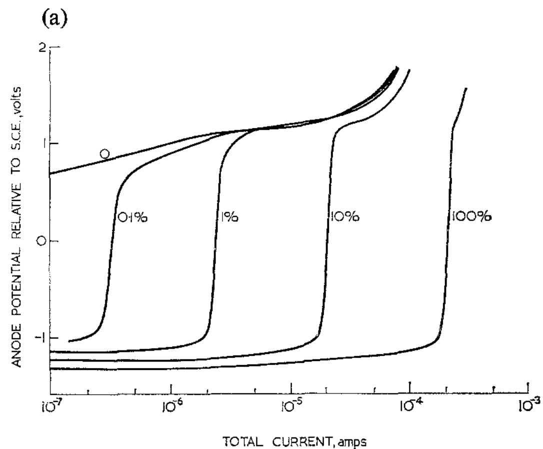

(b)

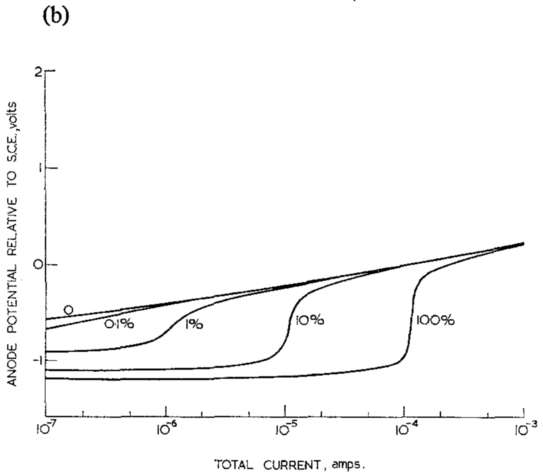

(c)

Fig. 4. Voltage-current characteristics in the dark, and for various illumination intensities using 36 W tungsten lamp: (a) Sample No. 2; (b) Sample No. 4; (c) Sample No. 12.

Table 1

Sample No.	Supplier	Ingot No.	Dopant	Carrier concentration n (Hall) electrons cm^{-3}	Electron mobility μ_n (Hall) $cm^2 V^{-1} s^{-1}$	αW_1	αL_P	Carrier concentration n (Electrochem.) electrons cm^{-3}	Hole diffusion length L_P μm	Hole mobility μ_P $cm^2 V^{-1} s^{-1}$	Hole lifetime τ_P seconds
1	MON	G5–83	None	$3{\cdot}90\times10^{14}$	5520						
2	MON	EPI-Layer									
		03–0161–61	Te	$3{\cdot}75\times10^{15}$	6525	1·11	1·90	$3{\cdot}75\times10^{15}$	0·98	346	$1{\cdot}09\times10^{-9}$
3	B&H		None	$3{\cdot}07\times10^{16}$	4820	0·42	1·85	$2{\cdot}63\times10^{16}$	0·95	261	$1{\cdot}36\times10^{-9}$
3A	B&H		None	$3{\cdot}07\times10^{16}$	4820	0·77	1·20	$7{\cdot}80\times10^{15}$	0·62	261	$5{\cdot}78\times10^{-10}$
4	MCP	A1082	None	$3{\cdot}81\times10^{16}$	4700	0·42	0·56	$2{\cdot}63\times10^{16}$	0·29	255	$1{\cdot}29\times10^{-10}$
5	MCP	X2298	Si	$8{\cdot}76\times10^{16}$	3600	1·07	0·51	$4{\cdot}04\times10^{15}$	0·26	200	$1{\cdot}33\times10^{-10}$
6	MCP	AX656A	Sn	$9{\cdot}60\times10^{16}$	3360						
7	MCP	X2035	Te	$2{\cdot}66\times10^{17}$	3280	0·19	0·52	$1{\cdot}28\times10^{17}$	0·27	184	$1{\cdot}55\times10^{-10}$
8	B&H		Si	$3{\cdot}76\times10^{17}$	3510	0·18	1·62	$1{\cdot}43\times10^{17}$	0·84	196	$1{\cdot}42\times10^{-9}$
9	MCP	X2382	Te	$6{\cdot}49\times10^{17}$	2860	0·26	1·03	$6{\cdot}85\times10^{16}$	0·53	163	$6{\cdot}77\times10^{-10}$
10	MCP	X2044	Si	$7{\cdot}73\times10^{17}$	2950	0·32	1·53	$4{\cdot}50\times10^{16}$	0·79	169	$1{\cdot}45\times10^{-9}$
11	RRE	A247	Si	$9{\cdot}90\times10^{17}$	2240	0·115	0·31	$3{\cdot}50\times10^{17}$	0·16	125	$8{\cdot}03\times10^{-11}$
12	MCP	X1978	Si	$1{\cdot}90\times10^{18}$	2100	0·123	0·34	$3{\cdot}06\times10^{17}$	0·17	114	$9{\cdot}95\times10^{-11}$
13	RRE	A289	Si	$1{\cdot}92\times10^{18}$	1690	0·175	0·17	$1{\cdot}52\times10^{17}$	0·08	79	$3{\cdot}18\times10^{-11}$

3. Results

3.1. *Voltage-current characteristics*

The properties of thirteen samples whose electrochemical voltage-current characteristics were investigated are listed in Table 1.

Fig. 3 illustrates the typical dependence of voltage-current characteristics upon sample doping level, by comparing three samples: No. 2, lightly doped ($3{\cdot}75\times10^{15}$ cm^{-3}), No. 4, medium doped ($3{\cdot}81\times10^{16}$ cm^{-3}), and No. 12, heavily doped ($1{\cdot}90\times10^{18}$ cm^{-3}). It should be noted that absolute current, not current density, is plotted; the exposed sample area was 0·07 cm^2. Characteristic plots are shown both for the samples in the dark, and under steady illumination; the dark current of the low-doped sample did not fall within the potential range explored. The illumination source for this set of experiments was the potassium discharge lamp, which was preferred to a tungsten lamp for the purposes of subsequent analysis according to the model to be described below.

The characteristic plots shown in Figs. 4a, b and c, show the effect of varying the illumination intensity over a range of three orders of magnitude for the same three samples. For the purposes of this experiment it was necessary to use the 36 W tungsten lamp in order to obtain sufficiently intense illumination; the intensity was varied by means of neutral density filters.

An analysis of the above results is attempted in Section 4·3; however some observations on electrochemical stripping of epitaxial layers will be given first.

3.2. *Epitaxial layer measurements*

The change in anodic voltage-current characteristics of an epitaxial layer structure (n on n$^+$), as the layer was removed by anodic dissolution, is shown in Fig. 5. In this case, the layer was supplied by RRE (Layer No. $SN_{11}R_{30}B$), and according to the supplier, consisted of material with an electron concentration 9×10^{15} cm^{-3} and mobility 4540 cm^2 V^{-1} s^{-1}, with thickness 5 to 8 μm, on a substrate with carrier concentration approximately 10^{18} cm^{-3}, and mobility about 2000 cm^2 V^{-1} s^{-1}. The numbers marked on the diagram represent the depth of material removed (in μm) at the stage when each curve was plotted; as previously indicated this is known from the time integral of dissolution current, since, in general, the mass of material removed electrolytically is given by $m = \frac{M}{nF}\int I\,dt$ where M is the molecular weight of the compound, F is the Faraday, and n the number of charge carriers involved in the dissolution reaction.

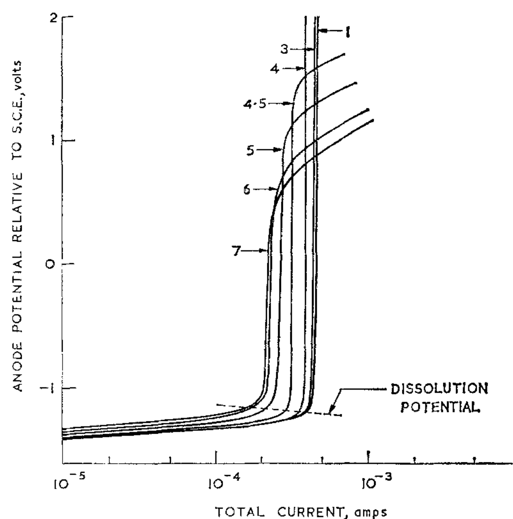

Fig. 5. Voltage-current characteristics as a function of depth removed during the anodic dissolution of an epitaxial layer, sample No. SN_{11} R_{30} B.*

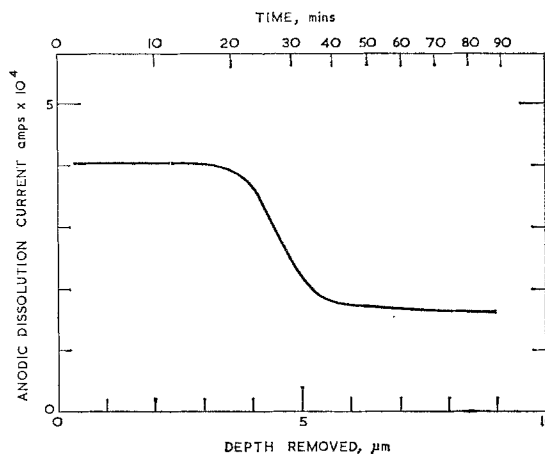

Fig. 6. Dissolution current as a function of depth removed, and time, during the anodic dissolution of the epitaxial layer referred to in Fig. 5.

* The numbers represent the depth removed, in μm.

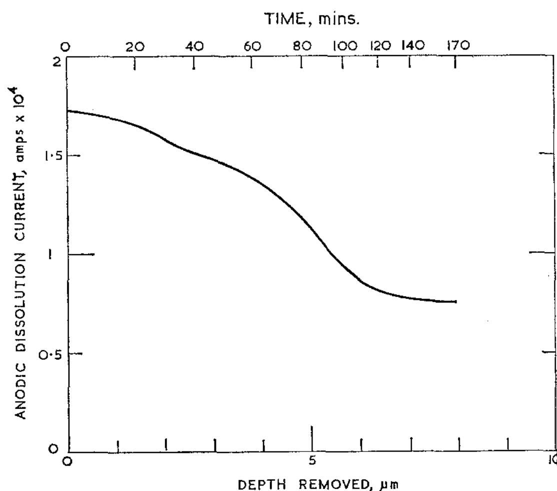

Fig. 7. Dissolution current as a function of depth removed, and time, during the anodic dissolution of a double epitaxial layer structure, sample No. JJ 101A.

Weight loss measurements have confirmed that $n = 6$ for the GaAs reaction [9].

It should be noted that the dissolution was performed with the sample under strong illumination, and with the dissolution potential maintained well below that at which the dark current intrusion was apparent for the substrate. (The small variation of dissolution potential with current occurred because it differed from the potentiostat control potential, by the amount of the voltage drop at the current-carrying probe contact to the substrate. This was due to the need for grounding the external voltage sweep source, and does not represent a malfunction of the potentiostat.) The anodic current during dissolution as a function of depth removed under these conditions is shown in Figure 6. A correlation between these results, and the supplier's figure for the layer thickness is apparent.

A similar plot for a double epitaxial layer (n-n-n^+) structure appears in Fig. 7. The sample was No. JJ 1021A, provided by the Plessey company and specified as a 2 μm thick layer, carrier concentration 7×10^{15} cm^{-3}, on a 4 μm thick intermediate layer with concentration about 10^{17} cm^{-3}, on a substrate with concentration about 10^{18} cm^{-3}. Again the correlation is obvious.

The use of much higher anode dissolution potentials, above the upper knee of the substrate characteristics has also been investigated, where the current *increases* as the heavily doped substrate is approached. It has been found, however, that the high 'dark' currents in this region tend to be relatively unstable, and furthermore that pitting of the substrate occurs under these conditions, as depicted in Fig. 8. Dissolution at the lower anode potentials maintained a polished surface, with topographic details which are believed to be associated with structural imperfections in the layer or substrate, as shown in Figs. 9, 10 and 11. (Figs. 8 and 11 refer to layers $SN_{11}R_{30}C$ and $SN_{11}R_{30}B$ (having similar specifications) and Figs. 9 and 10 refer to sample JJ 1021A; note that we have specifically sought to depict areas showing topographical features and that these samples by no means represent the current state of the art of layer growth reached by the suppliers.)

4. Analytical treatment of results

4.1. *Model for analysis*

Quantitative analysis will be confined to the behaviour under illumination; the dark current behaviour will be discussed briefly in a later section. The well-defined current-limited region apparent in all curves for n-type samples under illumination (up to the point at which dark current intrudes), and during anodic polarization, indicates that minority carriers (holes) are involved in the charge transfer reaction [7]. The model developed by Gaertner [10] to describe the photo-effect at a reverse-biased metal-semiconductor or p-n junction surface barrier provides a basis for the analysis of this behaviour, as discussed by Myamlin and Pleskov [6].

The main feature of the model, as shown in Fig. 12, is a depletion region, width W, beyond which lies a quasi-neutral diffusion region, width L_p, the minority carrier diffusion length. Light incident at the surface is absorbed according to a coefficient α, such that the light energy dissipated per unit length, $g(x)$ is $\Phi \alpha \exp(-\alpha x)$ where Φ is the intensity of total light flux absorbed. It is assumed that electron-hole pairs are generated, both in the depletion region and the diffusion region, according to the function $g(x)$; recombination and thermal generation in the depletion region are neglected. Thus the photo-

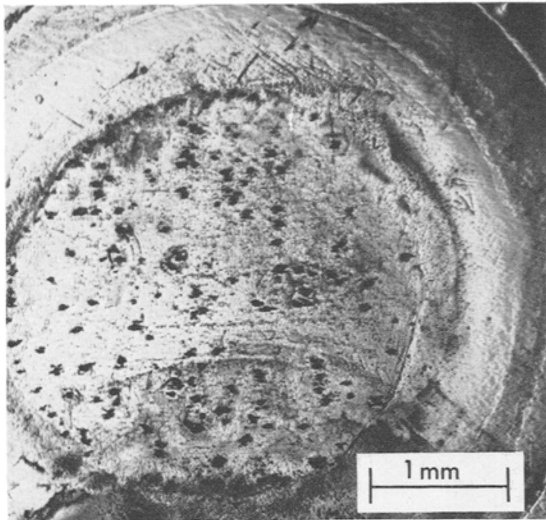

Fig. 8. Pitting observed after the dissolution of an epitaxial layer at high anodic potential (+0·6 V relative to S.C.E.).

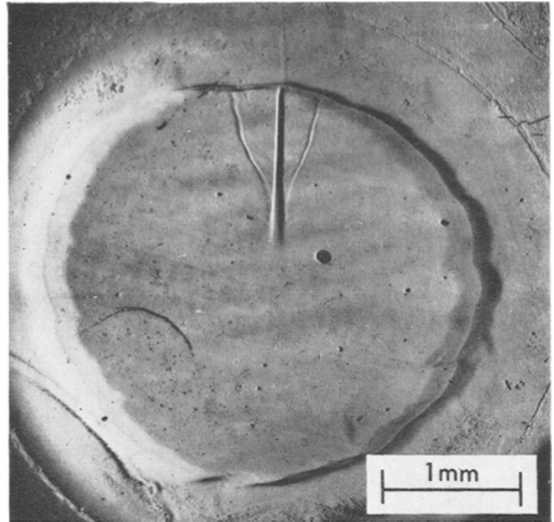

Fig. 9. Smooth substrate with a few defects revealed by the dissolution of the epitaxial layer at low anodic potential (−0·8 V relative to S.C.E.).

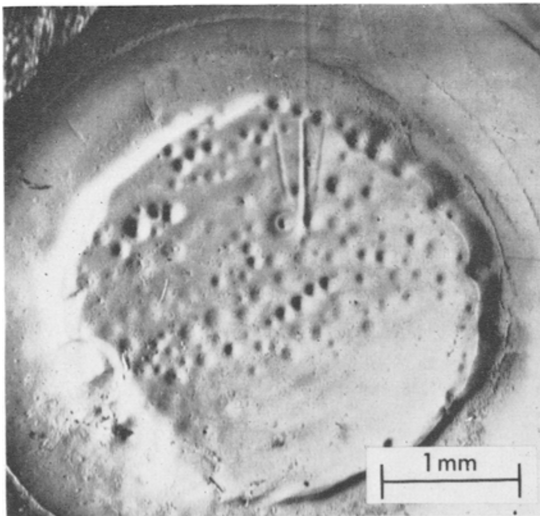

Fig. 10. Small areas resistant to etching at low anodic potential (−0·8 V relative to S.C.E.).

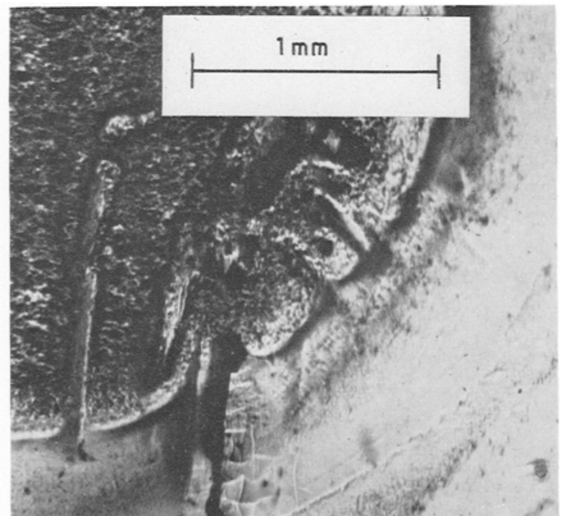

Fig. 11. Larger areas resistant to etching at low anodic potential (−0·8 V relative to S.C.E.).

facing p. 6

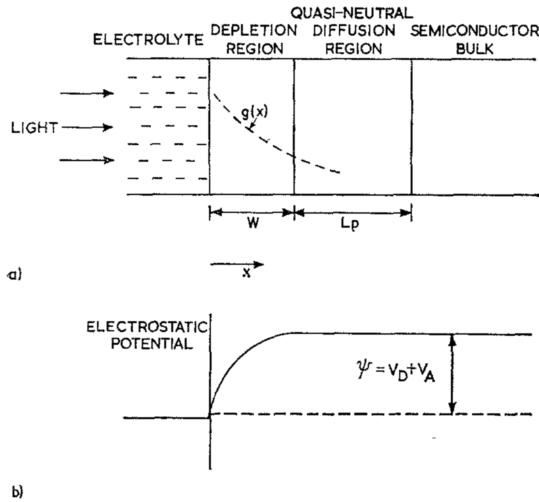

Fig. 12. (a) Model for the derivation of the photoeffect after Gaertner [10] and Myamlin and Pleskov [6]; (b) Corresponding electrostatic potential as a function of depth.

current density J, consists of two components: J_{depl}, the drift current density due to holes generated within the depletion region, and J_{diff}, due to holes generated within the quasi-neutral region and diffusing into the depletion region.

These contributions are given by:

$$J_{depl} = q\,\Phi\,[\exp(-\alpha W)-1] \tag{1}$$

and
$$J_{diff} = -q\,\Phi\left[\frac{\alpha L_p \exp(-\alpha W)}{1+\alpha L_p}\right] \tag{2}$$

where q is the electronic charge.

(An additional term, given by Gaertner, which would appear in Equation 2 is always negligible in our work, where $n \gg p$, and has been neglected.)

Thus the total photocurrent is:

$$J = -q\,\Phi\left[1-\frac{\exp(-\alpha W)}{1+\alpha L_p}\right] \tag{3}$$

The depletion region width W, is a function of the height of the potential barrier ψ between the surface and the interior of the semiconductor, and of the space charge density within the region. As indicated in the Fig. 12b, ψ is given by

$$\psi = V_D + V_A \tag{4}$$

where V_D is the equilibrium diffusion potential barrier between the semiconductor and electrolyte, and V_A is the externally measured anodic overvoltage. We have taken the space charge density to be $q(N_D{}^+ - N_A{}^-)$, where $N_D{}^+$ is the density of ionized donors and $N_A{}^-$ is the density of ionized acceptors, i.e. mobile charge carriers are neglected; the space charge density is thus numerically equal to the equilibrium net carrier concentration n. For $\psi \gg \frac{KT}{q}$, W is simply derived [11] to be:

$$W = W_1\,\psi^{\frac{1}{2}} \tag{5}$$

where

$$W_1 = \left(\frac{2\,\varepsilon\,\varepsilon_0}{qn}\right)^{\frac{1}{2}} \tag{5a}$$

where ε is the dielectric constant, and ε_0 is the permittivity of free space.

Thus from Equations 3 and 5, the current-voltage characteristic is given by:

$$J = -q\,\Phi\left[1-\frac{\exp(-\alpha W_1\,\psi^{\frac{1}{2}})}{1+\alpha L_p}\right] \tag{6}$$

or
$$I = -q\Phi A\left[1-\frac{\exp(-\alpha W_1\,\psi^{\frac{1}{2}})}{1+\alpha L_p}\right] \tag{7}$$

where current $I = JA$
where A = area of sample.

The effect of certain simplifications used in the derivation of Equation 6 should be pointed out. Tyagai [12] has shown that if a boundary condition ($p = 0$ at $x = W$), used in Gaertner's derivation of Equation 2, is avoided, a further parameter l (determined by effective carrier velocity and lifetime under specific conditions) has to be considered. In this case the term αL_p in Equations 6 and 7 should be replaced by β, where

$$\beta = \frac{L_p}{1+\frac{L_p}{l}+\frac{\alpha L_p{}^2}{l}} \tag{8}$$

Note that the correction becomes negligible for $l \gg L_p$. In any case, Equation 6 must become invalid for very small values of ψ, because for finite values of αL_p a discontinuity at $\psi = 0$ is implied (although substitution of β for αL_p would enable this difficulty to be overcome, provided

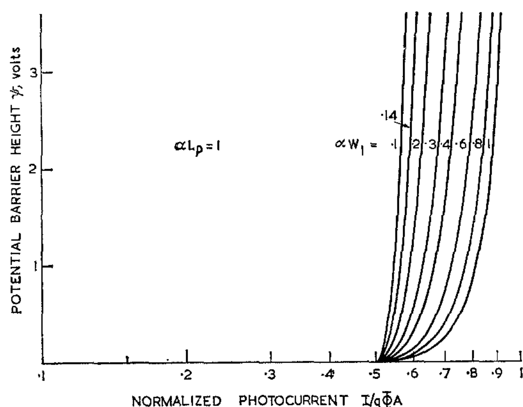

Fig. 13. Theoretical voltage-current curves for $\alpha L_p = 1$, and various values of αW_1.

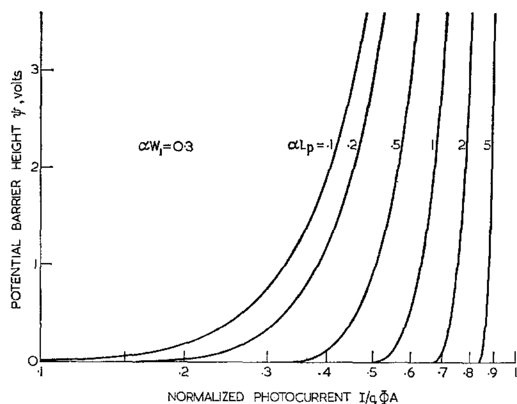

Fig. 14. Theoretical voltage-current curves for $\alpha W_1 = 0{\cdot}3$, and various values of αL_p.

that $I \rightarrow 0$ as $\psi \rightarrow 0$); also the use of Equation 5 in the derivation places a restriction on the application of the equation for small values of ψ.

With the above reservations in mind, the application of the above analysis to the experimental voltage-current characteristics was pursued. Fig. 13 shows Equation 7 plotted in the form ψ versus $I/q\ \Phi\ A$, for a constant value of αL_p and a range of values of αW_1. It is clear that, for constant αL_p, and ψ, the theoretical saturation photocurrent $q\ \Phi\ A$ is approached more closely by samples with the largest values of αW_1, i.e., with the lowest doping levels. Fig. 14 shows the effect for a constant value of αW_1 and varying values of αL_p; for the largest values of αL_p, the theoretical saturation current is more rapidly approached.

4.2 *Applicability to gallium arsenide electrode studies*

From Figs. 13 and 14 it is obvious that if αL_p and αW_1 were sufficiently large for all samples it would be difficult to resolve adequately the effects of changing doping levels, and hole diffusion lengths; thus a small value of α is desirable in practice. Experimentally the absorption coefficient α depends upon the photon energy of the incident light for a given material; this is shown in Fig. 15, due to Hwang [13], for gallium arsenide with an additional extrapolation between 1·60 and 1·65 eV. Close to the absorption edge, α depends somewhat on the doping level of the material, the curves being shifted to the right for material containing the highest impurity concentration. In Hwang's work the most heavily doped sample had a carrier concentration of $6{\cdot}5 \times 10^{18}$ electrons cm^{-3}. Thus the optimum experimental choice for α would appear to be that corresponding to a photon energy of about 1·62 eV, i.e., yielding as small as possible a value of α without it being doping level dependent. A potassium discharge lamp, with major emission lines at 766·5 nm and 769·9 nm, and corresponding photon energies of 1·617 eV and 1·610 eV was selected as the most suitable light source. A value of α of $1{\cdot}94 \times 10^4\ cm^{-1}$ (within 5 %) was deduced from the extrapolation of Hwang's results (Fig. 15).

4.3. *Analysis of experimental voltage-current data*

The following procedure was adopted to fit

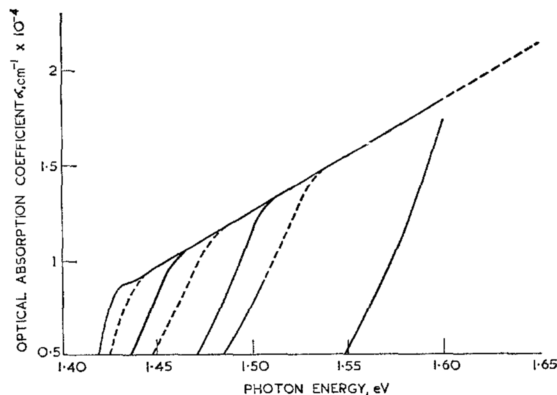

Fig. 15. Optical absorption coefficient α as a function of photon energy, at 300 K, for gallium arsenide samples with different doping levels, after Hwang [13], with an additional extrapolation from 1·60 to 1·65 eV.

theoretical curves, given by Equation 7, to experimental voltage-current plots taken under conditions of potassium-lamp illumination. Experimental curves were plotted with current on a 1 cycle logarithmic scale, for this analysis, as well as on the 4-cycle logarithmic scale shown in Fig. 3. It was decided to fit a curve to sample No. 2 (chosen because of a complete absence of dark current in the range studied and because this was epitaxial material having a high degree of structural perfection), assuming the value of αW_1 given by the known carrier concentration. The value of electrode potential corresponding to $\psi = 0$ was not known exactly, but was estimated roughly on the following basis; for the range of thirteen samples studied, a tendency for the anodic voltage, at the minimum current, to approach a lower limit, under increasingly intense illumination, has been observed. An ultimate limit would be expected to be reached, under sufficient optical excitation at the point defined by $\psi = 0$, i.e., $V_A = -V_D$; the value of the latter should not differ significantly between samples having the range of doping levels investigated. Thus, for a first approximation, in the analysis of all samples, the lowest anodic potential recorded in the entire batch (−1·34 volts relative to SCE for sample No. 8) was taken to represent the point $\psi = 0$ on the voltage axis. The final curve fitted to the experimental curve for sample No. 2 is shown in Fig. 16a; an excellent fit was obtained over the range $\psi >$ 0·4 V (i.e., about $15 \frac{KT}{q}$). From the curve it was possible to deduce the value of αL_p, and the saturation current $I_{sat} = q\, \Phi\, A$.

In order to predict carrier concentration n, and hole diffusion length L_p, for the remaining samples it was assumed that the same value of saturation current applied to all samples investigated, under the same conditions of illumination; the value of $2{\cdot}16 \times 10^{-5}$ A implied by the experiment on sample No. 2 was used. In each case trial values of αW_1 and αL_p for curve fitting were obtained by comparing experimental curves with sets of theoretical curves similar to those shown in Fig. 13, each set corresponding to a different value of αL_p. Final curve fitting was obtained by plotting further theoretical curves until the most acceptable fit was obtained; all were plotted using a programmed calculator and x-y plotter. The uncertainty in obtaining the best fit typically led to an uncertainty of less than about ±7% in αL_p and αW_1, and hence about ±15% in n, neglecting other sources of error. Fitted curves for samples 4 and 12 are in Figs.

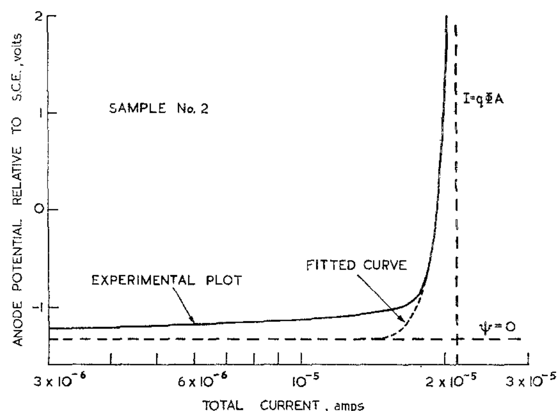

(a)

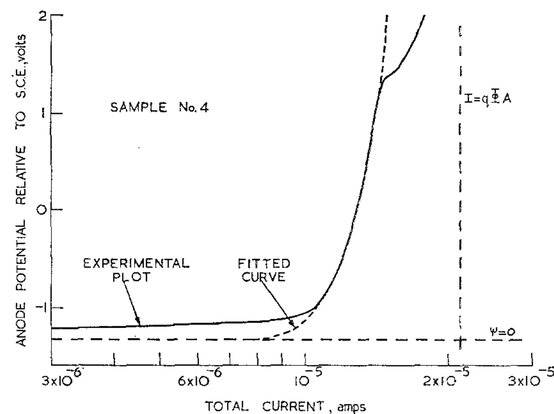

(b)

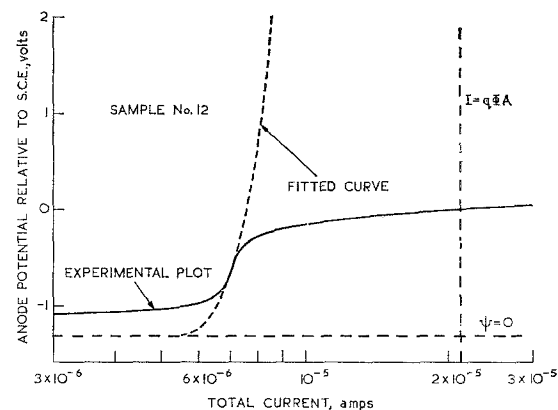

(c)

Fig. 16. Theoretical voltage-current curves fitted to experimental plots: (a) Sample No. 2; (b) Sample No. 4; (c) Sample No. 12.

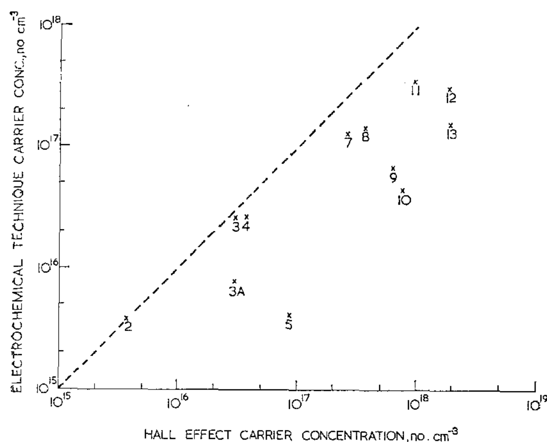

Fig. 17. Carrier concentration determined by the electrochemical technique versus carrier concentration measured by the Hall effect.

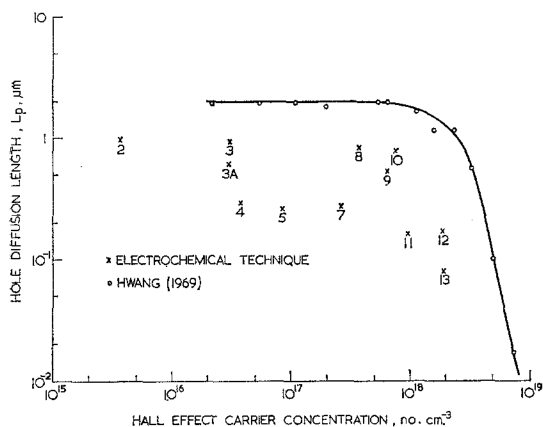

Fig. 18. Hole diffusion length determined by the electrochemical technique versus carrier concentration measured by the Hall effect. The data of Hwang [13] are shown for comparison.

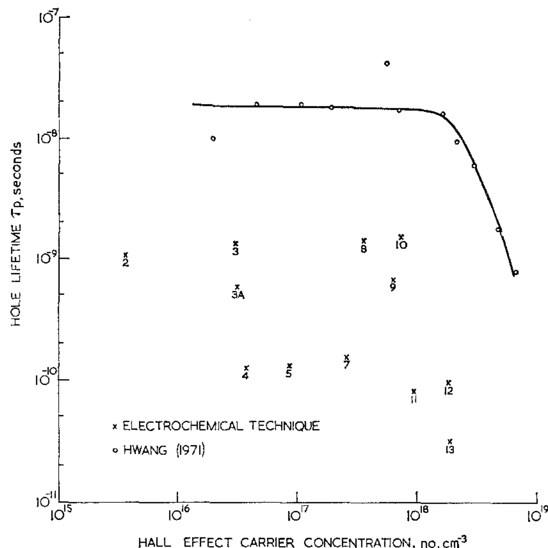

Fig. 19. Hole lifetime, determined by a combination of the electrochemical technique and Hall effect measurements. Hwang's data [15] are shown for comparison.

16b and 16c; the reliability of the procedure in the case of sample 12 and other very heavily doped samples is clearly suspect and will be discussed at a later point. The values of αW_1 and αL_p deduced from similar curves for all samples are shown in Table 1. Two sets of results appear for sample 3 for which voltage-current curves were taken on two separate occasions. (It was not possible to fit acceptable curves to the experimental curves for samples 1 and 6; their untypical shape was determined by the intrusion of an unusually high dark current.)

The carrier concentrations, implied by the values of αW_1, are also given in Table 1, and plotted in Fig. 17 against the previously measured values for the range of samples. All points should ideally lie on the broken line indicated; the point for sample 2 lies on the line since its known value of carrier concentration was assumed in the original curve fitting. There is a moderate agreement with the ideal behaviour in several cases, but one or two unexpected results are apparent. Values of the hole diffusion length L_p are plotted against carrier concentration in Fig. 18, and compared with results obtained by Hwang [13], on Te-doped gallium arsenide, using a combination of optical absorption and photoluminescence measurements.

An estimate of hole lifetime τ_p has also been obtained, using the relation $L_p = \sqrt{\tau_p D_p}$ where the hole diffusion coefficient is $D_p = \frac{KT}{q} \mu_p$. The evaluation requires a knowledge of the hole mobility μ_p; approximate values have been deduced from the measured electron mobility μ_n, from a plot of μ_p (in p-type material) versus μ_n (in n-type material) at fixed values of carrier concentration based on data published by Sze *et al* [14]. Values of τ_p thus obtained are plotted in Fig. 19, and once again a comparison is made with the results of Hwang [15] who used a photoluminescence phase shift technique.

5. Discussion

An aspect of the results which is dealt with only very briefly here, but which is apparent in the results for all but the most lightly doped samples, is the 'dark' current. Pleskov [16] has reported a similar effect in gallium arsenide, and proposes avalanche or tunnelling breakdown mechanisms, due to high surface field strengths (which for a given applied voltage increase rapidly with increasing carrier concentration). No detailed attempt has been made in this work to explore the dark current effect or to exploit its relationship with carrier concentration, as yet; in general the behaviour has been less reproducible than that under illumination.

The degree of success in relating Gaertner's model to our experimental data will now be discussed. The curves of Fig. 4, showing the dependence of photocurrent on light intensity, are of interest. The linear relationship between current (approaching the saturation level) and light intensity is in accordance with the model; note, however, the apparent change in shape of the voltage-current curves at low illumination intensity as the 'dark' current assumes importance.

It is clear, from Fig. 17, that the values of carrier concentration determined by curve fitting, according to the model, show in general a degree of quantitative agreement with values obtained by independent measurements. The values of L_p, thus obtained (Fig. 18), are also roughly of the same order as published results (though a systematic error by a factor of about two is suggested), which further supports the validity of the model. (Minority carrier diffusion length L_p, is an extremely useful parameter as an indication of material quality, as well as being a frequently used transistor device parameter.) The predicted values of minority carrier lifetime, τ_p (Fig. 19), compare less favourably with published work; however it must be appreciated that errors in L_p are amplified in the computation of τ_p and that the method of calculation used was merely a first approximation relying upon majority carrier mobility data.

A closer consideration of the results for carrier concentration is warranted, since we feel that despite one or two puzzling results the overall picture is most encouraging. There is an obvious tendency for carrier concentrations to be increasingly underestimated as the doping level increases; however, this can be understood in terms of the shapes of the experimental curves for the most heavily doped samples, such as that depicted in Fig. 16c. Reference to Fig. 4c suggests that the slope of the experimental curve is likely to be significantly less steep, in the region of curve fitting, because of the intrusion of dark current, than that which would be obtained under conditions of more intense illumination. This would result in an overestimate of αW_1 (see Fig. 13) and hence an underestimate of n, according to Equation 5a. Unfortunately the illumination intensity available from the monochromatic light source was rather limited, and it is intended to remedy this situation in future work. It was not feasible to correct numerically for the dark current with any degree of accuracy because of the very small slope of this characteristic. Other symptoms of experimental errors included observed long-term variations in the position of the experimental plots with respect to the reference zero potential, and changes of actual shape of the curves (e.g. in sample 3; compare points 3 and 3a), neither of which could be explained in terms of possible variations in light intensity.

Several possible sources of experimental error may be listed. These include spurious radiation, and instability, of the lamp, which might influence α, and, in the latter case, saturation photocurrent. Saturation photocurrent may also be influenced by variations in effective surface area, and reflectivity of samples. (In most cases the surface roughness factor is close to unity; for a hypothetical worst case, in which the crystal surface would be uniformly covered with etch-pits or pyramids, the factor would be close to 1·4.) The measured photocurrent may also be subject to the influence of surface states, and variations in these due to changes in surface morphology. The equilibrium surface potential could also be changed by these effects, and by variations within the electrolyte. Independent measurements have revealed variations in the mobility and carrier concentration within individual crystals investigated; these parameters

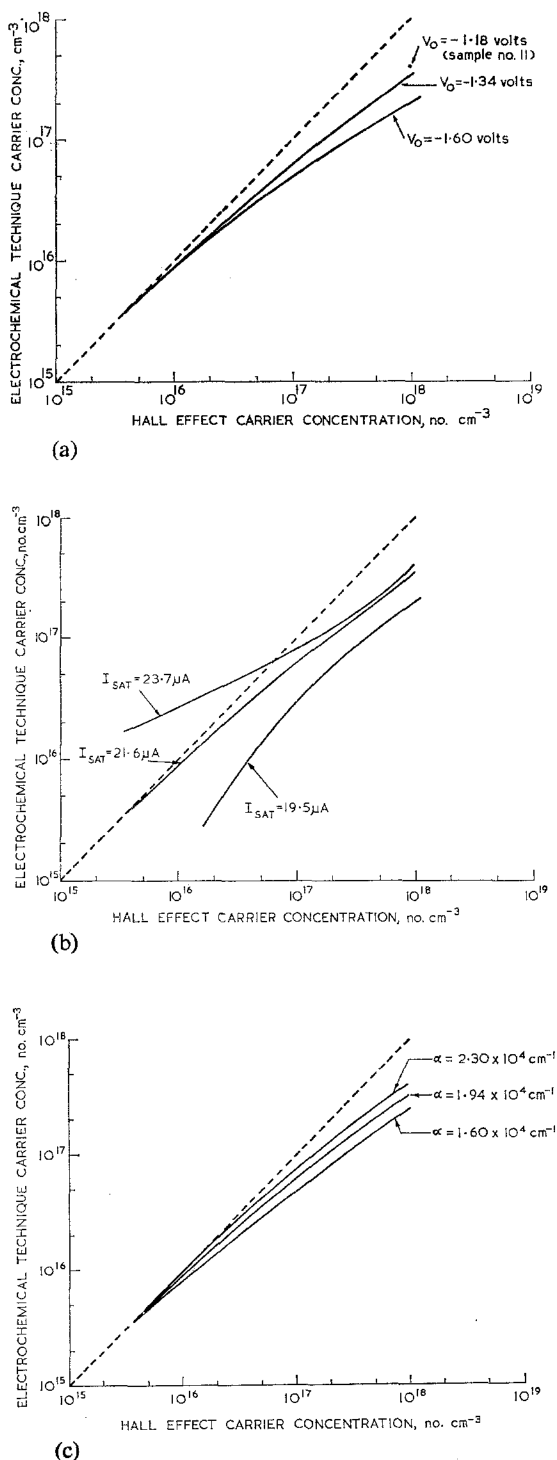

Fig. 20. Effect of variations in the curve-fitting technique on predicted values of carrier concentration: (a) Variations in the fixing point for $\psi = 0$; (b) Variations in the assumed saturation photocurrent; (c) Variations in the assumed optical absorption coefficient α.

will also vary with surface damage and ambient temperature. It has not been possible at this stage to examine all the above effects in detail, although it should be pointed out that only in the case of actual variations in carrier concentration and diffusion length (including variations with temperature) will the reproducibility of the *shape* of the voltage-current plots for a given sample be strongly influenced; air temperature variations of up to 8°C have been observed within the light-proof box, during the course of one day's experiments, so this must be regarded as a serious source of 'random' experimental error.

In addition to the experimental sources of error, the possible shortcomings of the model, and of our approach to the fitting of theoretical curves require further examination. Attention has already been drawn to certain limitations of the model; at this stage we shall only add that the implications of Equation 8 have been examined briefly, and we have estimated along the lines given by Tyagai [12], that $l/L_p > 10$ (except for $\psi \rightarrow 0$) throughout our work, so that no significant correction to αL_p should be required. In order to assess the systematic errors which could result from our fitting technique, several variations have been attempted, and the effects on the results for carrier concentration and hole diffusion length are summarized in Figs. 20 and 21. For clarity, data points are omitted, and the curves refer only to the relatively 'well-behaved' samples (2, 3, 4, 7, 8 and 10 in Fig. 20, and 2, 3, 8 and 10 in Fig. 21.) In Figs. 20a and 21a the effect is shown, of assuming that a lower anodic voltage relative to SCE, V_0, (i.e. $-1{\cdot}60$ V as compared with $-1{\cdot}34$ V) corresponds to the point $\psi = 0$; a small adjustment in the assumed value of saturation photocurrent (from 21·6 μA to 21·7 μA) was necessary to maintain the required fit to the 'standard' sample, No. 2. The effect of assuming a higher voltage, equal to the voltage at the minimum measured current for each individual sample, to define the point $\psi = 0$, was found only to have a noticeable effect in the case of the highest doped samples, as shown in Fig. 20a. Fig. 20b and 21b demonstrate the effect of assuming different values of saturation photocurrent (i.e. 21·6 μA $\pm \sim 10\%$) rather than fitting a value to suit the standard sample. In Figs. 20c and 21c the effect of assum-

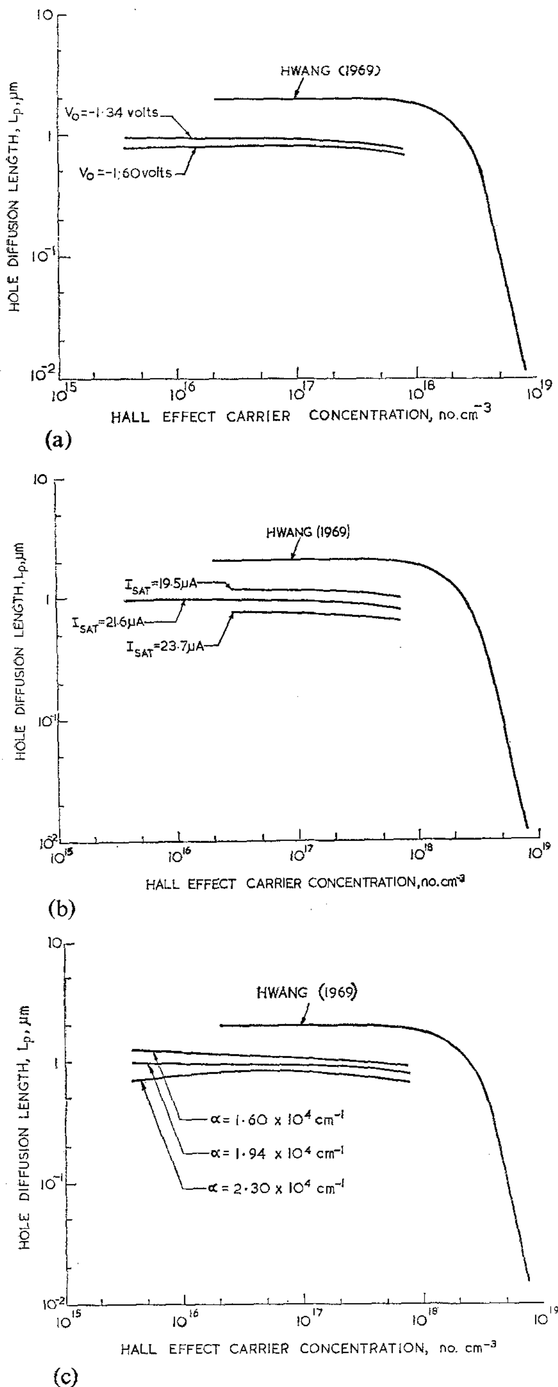

Fig. 21. Effect of variations in the curve-fitting technique on predicted values of hole diffusion length L_p. (a), (b) and (c), as for Fig. 20.

ing different values of the optical absorption coefficient α (i.e. $1{\cdot}94\times10^4\text{cm}^{-1}\pm\sim20\%$) is depicted; here the assumed value of saturation photo current was adjusted slightly (by $\pm\sim1{\cdot}5\%$ respectively) to retain a close fit to the standard sample. Generally the illustrated trends observed in the well-behaved samples were also seen in the remaining samples, none of whose data showed noticeable changes in position relative to that of their neighbours.

None of the above variations significantly improved the fit of experimental data simultaneously to the known values of carrier concentration and to the published values of hole diffusion length; this tends to confirm our belief that the most important source of systematic error in this work was the increasing intrusion of dark current with increasing doping level, at the illumination intensity used (although this still does not explain the discrepancy in the absolute values of diffusion length). We are confident that with further work, including optimisation and stabilisation of experimental conditions, and a more detailed consideration of theoretical behaviour, especially at low values of ψ (where the Gaertner [10] model is physically unrealistic) this method will prove to be a most attractive one for the measurement of carrier concentration, and minority carrier diffusion length.

Finally, we discuss the specific application of this work to the study of epitaxial n-type layers. Consideration of Gaertner's model indicates that the dissolution current at constant potential should begin to change, during etching, at the point where the thickness of the epitaxial layer remaining is equal to (L_p+W), and finally reach a constant value when the epitaxial layer has been completely removed. Thus the width of the transition region deduced from Fig. 6 indicates a value of about 2 μm for the hole diffusion length within the epitaxial layer, in good agreement with Hwang's data [13]. A useful feature of the anodic etching technique is that the exposure of topographical details, e.g. as shown in Fig. 11, provides qualitative information on the presence of electrical inhomogeneities, which will not be apparent from conventional measurements which average over a fixed area. Also, because the etching rate is carrier concentration dependent, the thickness uniformity of initially uneven, lightly doped, layers on heavily doped substrates is improved as the etching progresses towards the substrate, where the remaining layer thickness is less than

$(L_p + W)$; such thicknesses, of the order of 2 μm, are of interest in device manufacture. The application of the electrochemical method as a precision thinning technique for thicker layers is also of great interest, offering a degree of control which is unlikely to be matched by more conventional processes.

We are, in the present work, however, chiefly concerned with the accurate quantitative electrical assessment of relatively uniform layers. To date no detailed analysis of voltage-current curves, as a function of depth removed, has been attempted for epitaxial layers, but it should be pointed out that depth resolution should by no means be limited by the value of L_p as might be implied by Fig 6. Fig. 22 shows schematically the manner in which measured data would be plotted, assuming a layer structure with an abrupt carrier concentration profile as shown in part a. In plotting W, n, and L_p it is assumed that the measured values of αW and αL_p refer to the depth W below the surface at each stage; thus the depth resolution in carrier concentration measurement at the interface would be limited by W_{sub}. (This depletion width would be $\sim$0·02 μm (with ψ = 0·3 volts) for a substrate doping level of 10^{18} cm^{-3}, compared with W_{epi} $\sim$0·2 μm for an epitaxial layer doping level of 10^{16} cm^{-3}, and a hole diffusion length L_p up to $\sim$2 μm.) An independent estimate of L_p would also be obtained, which could be used to determine the absorption co-efficient α, if not already known.

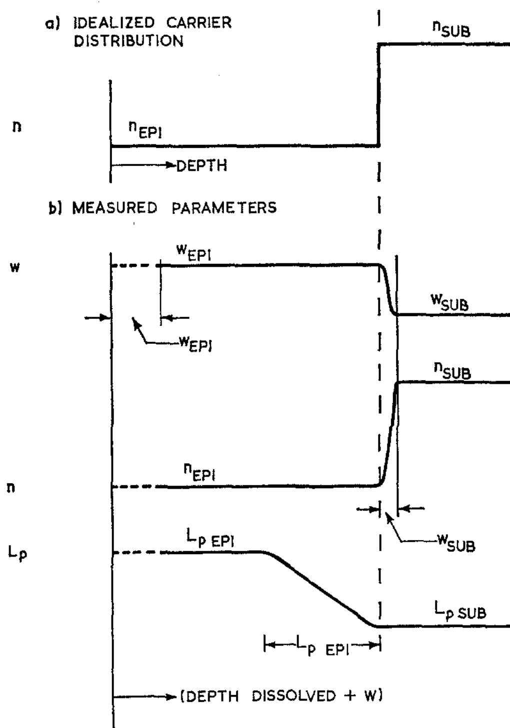

Fig. 22. Proposed analysis of epitaxial layer/substrate parameters as a function of depth.

6. Conclusion

The feasibility of using electrochemical techniques to determine the carrier concentration and minority carrier diffusion length of n-type gallium arsenide crystals has been demonstrated, and the extension to the measurement of depth dependence of these properties within epitaxial layers has been discussed. The techniques shows great promise as a practical system, and future work will be devoted to experimental improvements, and further theoretical studies, which, it is anticipated, will result in the construction of a fully automated profile plotter, with wide applicability to the assessment of high quality semiconductor materials for device applications.

Acknowledgments

Acknowledgment is made to E. Bremner for his contribution to the experimental work, including the design and construction of electronic units, and to the Director of Research of the Post Office for permission to publish this paper.

References

[1] P. Blood, *Acta Electronica*, **15** (1972) 33.
[2] Y. S. Lee and C. K. Kim, *Proc IEEE*, **58** (1970) 1153.
[3] D. J. Colliver, S. E. Gibbs and B. C. Taylor, *Electron Lett*, **6** (1970) 353.
[4] F. D. Hughes, *Acta Electronica*, **15** (1972) 43.
[5] P. J. Boddy, 'Progress in Solid State Chemistry' **4**, ed. by H. Reiss, Pergamon Press, Oxford (1967).
[6] V. A. Myamlin and Yu. V. Pleskov, 'Electrochemistry of Semiconductors', Plenum Press, New York (1967).
[7] H. Gerischer, 'Physical Chemistry—An Advanced Treatise: IX A Electrochemistry', chapter **5**, ed. by Eyring, Henderson, and Jost, Academic Press, New York (1970).
[8] M. V. Sullivan and G. A. Kolb, *J. Electrochem. Soc.*, **110** (1963) 585.
[9] H. Gerischer, *Ber. Bunsengesell. Phys. Chem.*, **69** (1965) 578.

[10] W. Gaertner, *Phys. Rev.*, **116** (1959) 84.
[11] A. Van der Zeil, 'Solid State Physical Electronics', 2nd Edition, Prentice-Hall, New Jersey (1968) 267.
[12] V. A. Tyagai, *Russian Journal of Physical Chemistry*, **38** (1964) 1335.
[13] C. J. Hwang, *J. Appl. Phys.*, **40** (1969) 3731.
[14] S. M. Sze, 'Physics of Semiconductor Devices', Wiley-Interscience, New York (1969) 40.
[15] C. J. Hwang, *J. Appl. Phys.*, **42** (1971) 4408.
[16] Yu. V. Pleskov, *Dokl. Akad. Nauk SSSR*, **143** (1962) 1399.